Preferential Cocrystallization among Distyrylbenzene Derivatives

Glenn P. Bartholomew, Xianhui Bu, and Guillermo C. Bazan*

Department of Chemistry, University of California, Santa Barbara, California 93106

Received September 27, 1999. Revised Manuscript Received May 13, 2000

A combination of powder and single-crystal X-ray diffraction techniques were used to probe the generality of phenyl−perfluorophenyl stacking among a small library of 1,4-distyrylbenzene derivatives. The specific derivatives in the present study are 1,4-bis-(4-dimethylaminostyryl)benzene (**DMADSB**), 1,4-distyrylbenzene (**DSB**), 1,4-di(1-cyano-2-phenylethenyl)-benzene(**CNDSB**), 1,4-di(1-cyano-2-(4-methylphenyl)ethenyl)benzene (**MeCNDSB**) 1,4-bis(styryl)-2,5-difluorobenzene (**2F$_c$**), 1,4-bis(4-fluorostyryl)-2,5-difluorobenzene (**2F$_c$2F$_t$**), 1,4-bis(pentaflourostyryl)benzene (**10F$_t$**), and 1,4-bis(pentafluorostyryl)-2,5-difluorobenzene (**2F$_c$10F$_t$**). Electrostatic distribution diagrams aid in assessing the likelihood of success in pair formation. Powder diffraction provides a means to determine both positive and negative results for binary phase formation. Four new structures are presented and discussed including (**DSB**/**2F$_c$10F$_t$**), (**DMADSB**/**2F$_c$10F$_t$**), (**CNDSB**/**2F$_c$10F$_t$**), and (**MeCNDSB**/**2F$_c$10F$_t$**). Single-crystal diffraction work confirms that the resulting lattices contain alternating layers of fluorinated and unfluorinated **DSB** derivatives arranged in a cofacial fashion with multiple H···F interactions between stacks. Differential scanning calorimetry is reported on (**DSB**/**2F$_c$10F$_t$**), (**CNDSB**/**2F$_c$10F$_t$**), (**MeCNDSB**/**2F$_c$10F$_t$**), and their components.

Introduction

Recently, considerable attention has been focused on the noncovalent interactions that organize organic molecules in the solid state.[1] This interest stems, in part, from the observation that the arrangement of molecules in the solid plays a critical role in determining the performance of organic materials in emerging optoelectronic technologies.[2] For example, the charge transport in organic field-effect transistors is affected by crystal size.[3,4] In thin film transistors based on fused thiophenes, appropriate intermolecular orientation leads to high charge mobility.[5] Advances in topochemical polymerizations show how the relative orientations of organic photoactive groups in the lattice can be optimized to facilitate a polymerization sequence across the crystal.[6] Altogether, these reports point to the need for strategies that optimize the relative orientations and distances in organic solids, especially in circumstances where hydrogen bonding is not an option.

Binary cocrystals, i.e., crystals with lattices containing complementary pairs of molecules, provide an interesting class of materials for gauging our understanding of intermolecular noncovalent interactions.[7] Formation of binary cocrystals occurs when the lattice containing both components is favored (kinetically or thermodynamically) over crystallization of the individual components.[8] From an applications perspective binary cocrystals are interesting because it should be possible to tailor the extent of through-space delocalization and the three-dimensional placement of individual components by finding complementary molecular sets.

In this contribution we focus on distyrylbenzene derivatives to probe the generality of phenyl−perfluorophenyl stacking as a means to obtain binary crystals.[9] Benzene and hexafluorobenzene are known to form a 1:1 complex in which the two compounds stack alternately in a face-to-face orientation.[10] It is commonly accepted that the driving forces for cocrystallization are electrostatic rather than charge-transfer interactions.[11,12] Cofacial stacking is also seen in the 1:1 complex of naphthalene and octafluoronaphthalene[13] as well as in the *trans*-decafluorostilbene and *trans*-stilbene pair.[6]

(1) (a) Philp, D.; Stoddart, J. F. *Angew. Chem., Int. Ed. Engl.* **1996**, *35*, 1154. (b) Stang, P. J.; Olenyuk, B. *Angew. Chem., Int. Ed. Engl.* **1996**, *35*, 732. (c) Desiraju, G. R. *Angew. Chem., Int. Ed. Engl.* **1995**, *34*, 2311. (d) Mascal, M. *Contemp. Org. Synth.* **1994**, *1*, 1. (e) Cram, D. J. *Nature* **1992**, *356*, 29. (f) Cram, D. J. *Angew. Chem., Int. Ed. Engl.* **1988**, *27*, 1009 and references therein.

(2) For earlier work on organic metals, see: Bryce, M. R.; Murphy, L. C. *Nature* **1994**, *309*, 119.

(3) Horowitz, G. *Adv. Mater.* **1998**, *10*, 365.

(4) Katz, H. E.; Lovinger, A. J.; Laquindanum, J. G. *Chem Mater.* **1998**, *10*, 457.

(5) Li, X.-C.; Sirringhaus, H.; Garnier, F.; Holmes, A. B.; Feeder, S. C.; Clegg, W.; Teat, S. M.; Friend, R. H. *J. Am. Chem. Soc.* **1998**, *120*, 2206.

(6) Coates, G. W.; Dunn, A. R.; Henling, L. M.; Ziller, J. W.; Labkovsky, E. B.; Grubbs, R. H. *J. Am. Chem. Soc.* **1998**, *120*, 3641.

(7) Etter, M. C.; Urbanczyk-Lipkowska, Z.; Zia-Ebrahimi, M.; Panunto, T. W. *J. Am. Chem. Soc.* **1990**, *112*, 8415.

(8) Etter, M. C. *J. Phys. Chem.* **1991**, *95*, 4601.

(9) (a) Coates, G. W.; Dunn, A. R.; Henling, L. M.; Dougherty, D. A.; Grubbs, R. H. *Angew Chem., Int. Ed. Engl.* **1997**, *36*, 248. (b) Patrick, C. R.; Prosser, G. S. *Nature* **1960**, *4742*, 1021. (c) Bruce, M. I.; Snow, M. R.; Tiekink, E. R. T. *Acta Crystallogr.* **1987**, *43*, 1640.

(10) Williams, J. H.; Cockcroft, J. K.; Fitch, A. N. *Angew. Chem., Int. Ed. Engl.* **1992**, *C31*, 1655.

(11) Cozzi, F.; Ponzini, F.; Annunziata, R.; Cinquini, M.; Siegel, J. S. *Angew. Chem., Int. Ed. Engl.* **1995**, *34*, 1019.

10.1021/cm990608a CCC: $19.00
Published on Web 07/14/2000

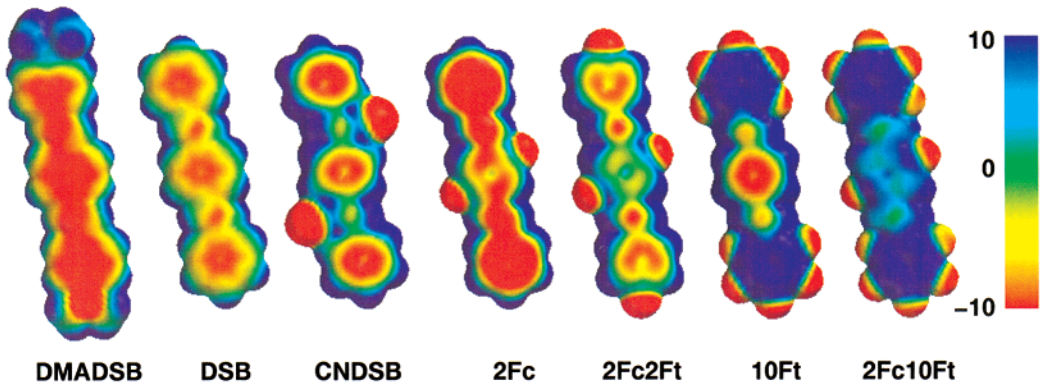

Figure 1. Electrostatic potential maps of **DMADSB**, **DSB**, **CNDSB**, $\mathbf{2F_c}$, $\mathbf{2F_c2F_t}$, $\mathbf{10F_t}$, **and** $\mathbf{2F_c10F_t}$. Scale shown is in units of kcal/mol.

The components of the present study include: 1,4-bis-(4-dimethylaminostyryl)benzene (**DMADSB**), 1,4-distyrylbenzene (**DSB**), 1,4-bis(styryl)-2,5-difluorobenzene ($\mathbf{2F_c}$), 1,4-bis(4′-fluorostyryl)-2,5-difluorobenzene ($\mathbf{2F_c2F_t}$), 1,4-bis(pentaflourostyryl)benzene ($\mathbf{10F_t}$), 1,4-bis(pentafluorostyryl)-2,5-difluorobenzene ($\mathbf{2F_c10F_t}$), 1,4-di(1-cyano-2-phenylethenyl)benzene (**CNDSB**), and 1,4-di(1-cyano-2-(4-methylphenyl)ethenyl)benzene (**MeCNDSB**). Molecules of this type have been studied previously because of their potential use as laser dyes,[14] their strong two-photon absorption properties,[15] and their morphological content in modeling electroactive polymers.[16,17]

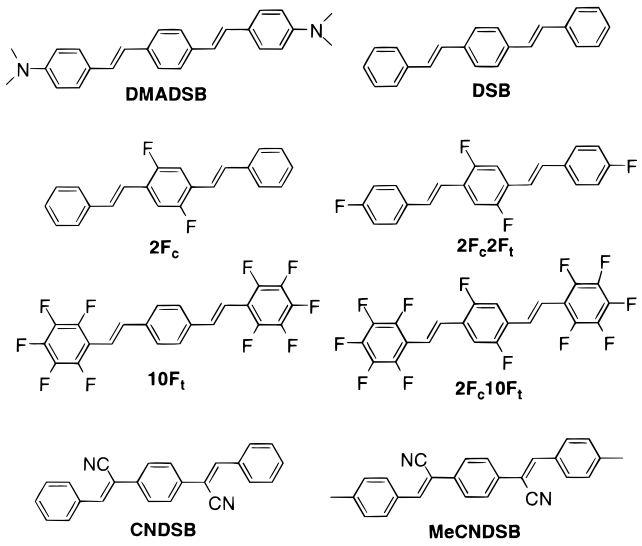

Results and Discussion

Electrostatic Distributions. Figure 1 contains the electrostatic distribution maps calculated for the compounds studied. These maps were calculated using the Spartan 5.0.1 computational package. After an ab initio geometry optimization was performed using the 3-21G basis set, single-point energy calculations were performed at the 6-21G level. Electrostatic potential surfaces were created for each molecule at high resolution for a density value of 0.002 electrons/au.[3] Red areas correspond to regions of partial negative charge, whereas blue surfaces highlight regions with partial positive charge. The molecules are shown on the same electrostatic potential scale for ease of comparison.

In **DSB**, a greater proportion of the partial negative charge is located within the volume of space above and below the center of the aryl rings and the olefin linkages. Addition of the electron donating dimethylamino groups increases the electron density within the core of **DMADSB**. Fluorine substitution in $\mathbf{2F_c10F_t}$ inverts the electrostatic distribution, leaving the inner portion of the ring with a partial positive charge. **DSB** and $\mathbf{2F_c10F_t}$ have been described as having complementary quadrupole moments that lead to an attractive interaction upon stacking.[18] The remaining molecules fall along a continuum between the two extremes of **DMADSB** and $\mathbf{2F_c10F_t}$, having a range of electron density within the core of the aromatic rings.

Figure 1 may serve as a starting point when potentially complementary pairs are being chosen. The pairs (**DSB**/$\mathbf{2F_c10F_t}$), (**DMADSB**/$\mathbf{2F_c10F_t}$), and ($\mathbf{2F_c}$/$\mathbf{10F_t}$) are obvious candidates, because these have the ability to juxtapose rings with inverted polarities. The pair (**CNDSB**/$\mathbf{2F_c10F_t}$) was chosen to examine components which have strong electron withdrawing groups, yet appear to have complementary surfaces. The (**MeCNDSB**/$\mathbf{2F_c10F_t}$) couple allows us to investigate the effect of a small steric perturbation on long-range packing when compared to (**CNDSB**/$\mathbf{2F_c10F_t}$). The binary sets (**DSB**/$\mathbf{2F_c2F_t}$), (**DSB**/$\mathbf{10F_t}$), (**DMADSB**/$\mathbf{2F_c2F_t}$), and (**DMADSB**/$\mathbf{2F_c}$) provide intermediate cases.

Powder Diffraction. X-ray powder diffraction (XRD) provides a convenient tool to determine which pairs lead to binary crystal formation. This technique can be used to detect and characterize new phases in inorganic systems[19] and to monitor the formation of organic

(12) (a) Cozzi, F.; Cinquini, M.; Annuziata, R.; Siegel, J. S. *J. Am. Chem. Soc.* **1993**, *115*, 5330. (b) Hunter, C. A.; Sanders, J. K. M. *J. Am. Chem. Soc.* **1990**, *112*, 5525. (c) Hunter, C. A. *Angew. Chem., Int. Ed. Engl.* **1993**, *32*, 1584. (d) Williams, V. E.; Lemieux, R. P.; Thatcher, G. R. J. *J. Org. Chem.* **1996**, *61*, 1927.

(13) Potenza, J.; Mastropaolo, D. *Acta Crystallogr.* **1975**, *B31*, 2527.

(14) Heller, A. *J. Chem. Phys.* **1964**, *40*, 2839.

(15) Albota, M.; Belijonne, D.; Bredas, J. L.; Ehrlich, J. E.; Fu, J. Y.; Heikal, A. A.; Hess, S. E.; Kogej, T.; Levin, M. D.; Marder, S. R.; McCord-Maughon, D.; Perry, J. W.; Rockel, H.; Rumi, M.; Subramaniam, C.; Webb, W. W.; Wu, X.-L.; Xu, C. *Science* **1998**, *281*, 1653.

(16) Bartholomew, G. P.; Bu, X.; Bazan, G. C.; Lachicotte, R. J. Submitted for publication in *Chem. Mater.* submitted.

(17) Renak, M. L.; Bartholomew, G. P.; Wang, S.; Ricatto, P. J.; Lachicotte, R. J.; Bazan, G. C. *J. Am. Chem. Soc.* **1999**, *121*, 7787.

(18) Brown, N. M. D.; Swinton, F. L. *J. Chem. Soc., Chem. Commun.* **1974**, 770.

(19) Langford, J. I.; Louër, D. *Rep. Prog. Phys.* **1996**, *59*, 131 and references therein.

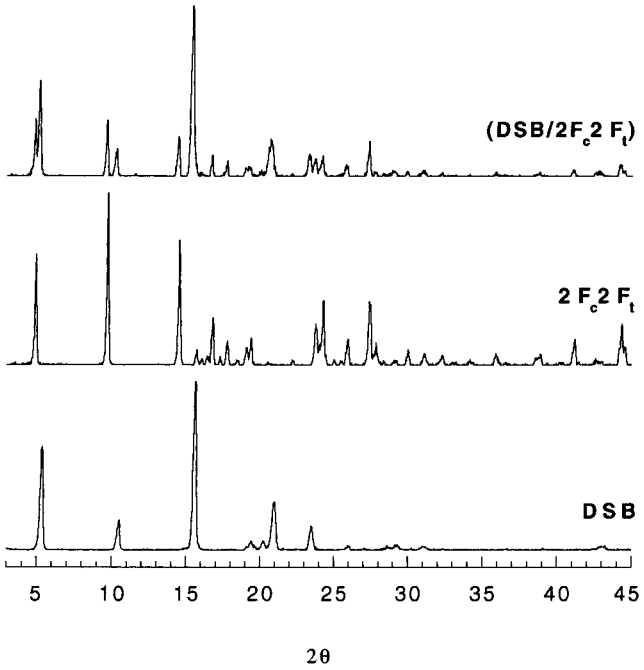

Figure 2. Comparison of X-ray powder diffraction patterns for the mixture of (**DSB**/**2F$_c$2F$_t$**) recovered from a THF solution with the single component scan of both **2F$_c$2F$_t$** and **DSB**. All intensities are scaled relative to the largest peak in each pattern.

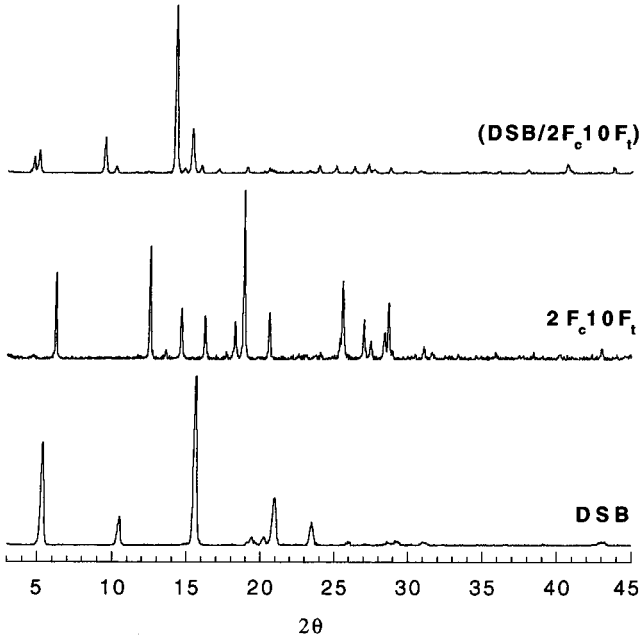

Figure 3. Comparison of X-ray powder diffraction patterns for the mixture of (**DSB**/**2F$_c$10F$_t$**) recovered from a THF solution with the single component scan of both **2F$_c$10F$_t$** and **DSB**. All intensities are scaled relative to the largest peak in each pattern.

cocrystals assembled by hydrogen bonding.[20] Samples were prepared by weighing equimolar amounts of both constituents for a total of 30−40 mg of total mixture. These solids were dissolved in tetrahydrofuran (THF) and the solvent was evaporated by flowing a stream of nitrogen over the solution. THF was chosen as the solvent on the basis of the solubility of the target components (vide infra). The resulting solids were then carefully collected and ground to a fine powder with an agate mortar and pestle.

A comparison of the diffraction patterns of **DSB**, **2F$_c$2F$_t$**, and (**DSB**/**2F$_c$2F$_t$**) is shown in Figure 2 and data for **DSB**, **2F$_c$10F$_t$**, and (**DSB**/**2F$_c$10F$_t$**) are shown in Figure 3. Visual inspection of the three patterns corresponding to the (**DSB**/**2F$_c$2F$_t$**) and components reveals no new peaks, whereas comparison of the (**DSB**/**2F$_c$10F$_t$**) mixture and components displays unique peaks for the mixture. The absence of new peaks argues against the formation of a cocrystal[19] from the (**DSB**/**2F$_c$2F$_t$**) solution, whereas the new peaks in the diffraction pattern of (**DSB**/**2F$_c$10F$_t$**) are a strong indication of a new phase and suggest attractive interactions between **DSB** and **2F$_c$10F$_t$**.[21]

By this method, it was established that the following pairs lead to binary crystal formation: (**DSB**/**2F$_c$10F$_t$**), (**DMADSB**/**2F$_c$10F$_t$**), (**CNDSB**/**2F$_c$10F$_t$**), and (**CNDSB**/**2F$_c$10F$_t$**). The following pairs are not compatible: (**2F$_c$**/**10F$_t$**), (**DSB**/**10F$_t$**), (**DSB**/**2F$_c$2F$_t$**), (**DMADSB**/**2F$_c$2F$_t$**), (**DMADSB**/**2F$_c$**), and (**DMADSB**/**DSB**). That (**2F$_c$**/**10F$_t$**) fails is surprising in light of the success with (**DSB**/**2F$_c$10F$_t$**) and the report by Grubbs that **10F$_t$** and *trans*,*trans*-1,4-bis(styryl)-2,3,5,6-tetrafluorobenzene (**4F$_c$10F$_t$**) cocrystallize.[6] Attempts to obtain cocrystals suitable for single-crystal XRD from solution were successful for all four mixtures, as indicated by XRD comparison. Similar efforts for those mixtures counterindicated by powder diffraction gave crystals that could be indexed to the individual components.

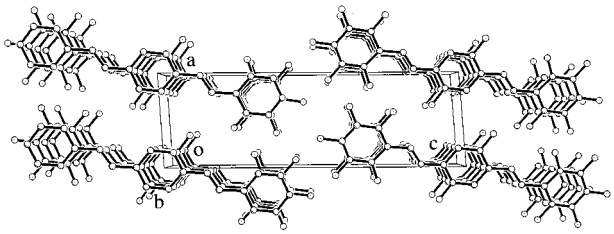

Figure 4. Molecular packing diagram of (**DSB**/**2F$_c$10F$_t$**) with a view down the *b* axis.

Single-Crystal XRD. Attempts to grow single crystals for diffraction studies of (**DSB**/**2F$_c$10F$_t$**) directly from THF proved to be unsuccessful. Suitable crystals formed when ethanol was allowed to diffuse over a period of 6 weeks into a solution containing a 1:1 ratio of **DSB** and **2F$_c$10F$_t$** in benzene. Figure 4 shows a packing diagram of the (**DSB**/**2F$_c$10F$_t$**) pair along the *b* axis and crystallographic parameters are listed in Table 1.[22] **DSB** and **2F$_c$10F$_t$** are stacked face-to-face with a transverse slip of 1.31 Å and a longitudinal slip of 0.60 Å (Figure 5). The average ring-to-ring distance between stacked molecules is approximately 3.42 Å. Multiple close contacts between F atoms on **2F$_c$10F$_t$** and adjacent H sites on **DSB** become apparent (F(6)···H−C(18) = 2.626(6) Å; F(5)···H−C(19) = 2.671(6) Å; F(1)·

(20) (a) Etter, M. C.; Reutzel, S. M.; Choo, C. G. *J. Am. Chem. Soc.* **1993**, *115*, 4411. (b) Caira, M. R.; Nassimbeni, L. R.; Wildervanck, A. F. *J. Chem. Soc., Perkin Trans.* **1995**, *2*, 2213. (c) Pedireddi, V. R.; Jones, W.; Chorlton, A. P.; Docherty, R. *Chem. Commun.* **1996**, 987.

(21) To address the possibility that the pattern of (**DSB**/**2F$_c$10F$_t$**) is a consequence of peak displacement from refocusing by different crystallite geometries or other systematic errors, a mixture of fine powders of DSB and **2F$_c$10F$_t$** were sifted together. All of the peaks in the resulting diffraction pattern can be traced to the data of DSB and **2F$_c$10F$_t$**. For more discussion, see: Jenkins, R.; Fawcett, T. G.; Smith, D. K.; Visser, J. W.; Morris, M. C.; Frevel, L. K. *Powder Diffr.* **1986**, *1*, 51.

Table 1. Crystal Data and Refinement Parameters for (DSB/2F$_c$10F$_t$), (DMADSB/2F$_c$10F$_t$), (CNDSB/2F$_c$10F$_t$), and (MeCNDSB/2F$_c$10F$_t$)

crystal parameters	(**DSB**/2F$_c$10F$_t$)	(**DMADSB**/2F$_c$10F$_t$)	(**CNDSB**/2F$_c$10F$_t$)	(**MeCNDSB**/2F$_c$10F$_t$)
chemical formula	$C_{44}H_{24}F_{12}$	$C_{48}H_{34}F_{12}N_2$	$C_{46}H_{22}F_{12}N_2$	$C_{48}H_{26}F_{12}N_2$
formula weight	780.63	866.77	830.66	858.71
crystal system	triclinic	monoclinic	triclinic	triclinic
space group (no.)	$P\bar{1}$(#2)	$P2_1/c$ (#14)	$P\bar{1}$(#2)	$P\bar{1}$(#2)
Z	1	2	1	1
a, Å	5.9290(6)	7.5651(7)	6.2273(11)	6.1987(12)
b, Å	7.5121(7)	6.0906(5)	7.3814(14)	7.3589(14)
c, Å	18.651(2)	41.862(4)	19.354(4)	20.440(4)
α, deg	90.844(2)	90	90.114(3)	87.079(3)
β, deg	94.341(2)	91.996(2)	98.852(3)	81.437(3)
γ, deg	91.757(2)	90	94.842(3)	85.874(3)
volume, Å^3	827.82(14)	1927.6(3)	875.8(3)	918.8(3)
ρ_{calc}, Mg/m^3	1.566	1.493	1.575	1.552
crystal dimens, mm	0.04 × 0.18 × 0.40	0.43 × 0.16 × 0.013	0.52 × 0.40 × 0.13	0.52 × 0.40 × 0.13
temperature, °C	−80	25	−80	−80
2θ range for data	2.0−50.0	2.0−50.0	2.0−50.0	2.0−50.0
total reflections	3486	8651	9455	8168
independent reflections	2214 [$R_i(F^2)$= 0.0211]	3315 [$R_i(F^2)$ = 0.0763]	4012 [$R_i(F^2)$ = 0.0258]	3223 [$R_i(F^2)$ = 0.0395]
no. of observed data	1656 ($I > 2\sigma(I)$)	1451 ($I > 2\sigma(I)$)	4012 ($I > 2\sigma(I)$)	3214 ($I > 2\sigma(I)$)
no. of parameters varied	396	283	271	281
μ, mm^{-1}	0.138	0.128	0.137	0.133
$R_1(F)$, $wR2(F^2)$, ($I > 2\sigma(I)$)	0.0506, 0.1360	0.0584, 0.1078	0.0408, 0.1216	0.0558, 0.1388
$R_1(F)$, $wR_2(F^2)$, all data	0.0670, 0.1484	0.1669, 0.1578	0.0522, 0.1329	0.0851, 0.1560
goodness-of-fit on F^2	1.011	0.910	1.072	0.960

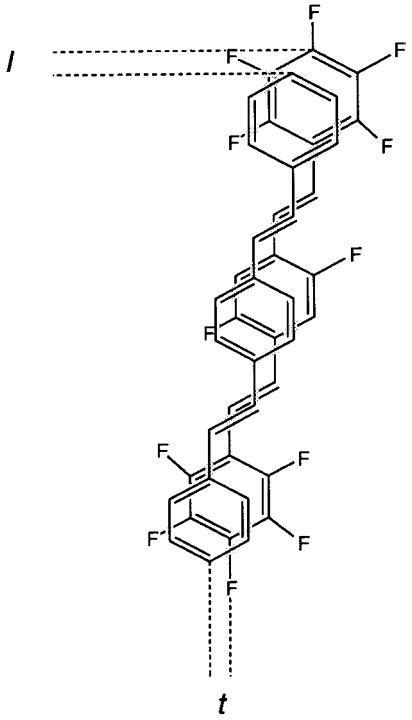

Figure 5. Illustration of transverse (t) slip and longitudinal (l) slip. Values calculated are t = 1.31 Å, l = 0.60 Å for (**DSB**/**2F$_c$10F$_t$**) and t = 1.43 Å, l = 0.86 Å for (**DMADSB**/**2F$_c$10F$_t$**).

··H−C(18) = 2.620(6) Å) (see Figure 6a).[23] These H···F interactions agree well with the electron distribution at the edges of the distyrylbenzene molecules and are consistent with recent findings by Desiraju that hydrogen bonding to fluorine is important in determining the crystal arrangements of fluorinated aromatic molecules.[24]

Both **DSB** and **2F$_c$10F$_t$** are located at the crystallographic inversion centers. **DSB**s are located at the edge centers of the b axis, whereas **2F$_c$10F$_t$** molecules are located at the unit cell origins. The long axes of both molecules are aligned approximately along the crystallographic c axis and the translation periodicity along the c axis is therefore determined by the length of the long molecular axis of **DSB** and **2F$_c$10F$_t$**.

The structure can also be considered to be built from layers stacked along the c axis. Such a structural feature is consistent with the platelike morphology of the crystal. Within each layer, **DSB** and **2F$_c$10F$_t$** form parallel columns. When viewed down the a axis, each column consists of molecules of the same type. However, when viewed down the b axis, molecules of different types alternate. It is of interest to examine the environment of each individual molecule. Within each layer, each **DSB** molecule is surrounded by two other **DSB** molecules at a distance that is equal to the a axial length (5.95 Å) and two **2F$_c$10F$_t$** molecules at a distance that is equal to half of the b axial length (3.80 Å). This seems to suggest that the interaction between molecules of the same type is comparable to the interaction of molecules of the different types. As a result, molecules of the same type are not completely insulated from each other.

Single crystals of (**DMADSB**/**2F$_c$10F$_t$**) suitable for crystallography were grown from a THF solution after

(22) A classic problem associated with single-crystal diffraction work is the possibility that the crystal chosen for structural study corresponds to a small amount of impurity and is not representative of the bulk sample. To verify that the single-crystal data were indeed representative of the powder morphology, the powder diffraction patterns were indexed against the unit cells determined from the single-crystal studies of (**DSB**/**2F$_c$10F$_t$**) and (**DMADSB**/**2F$_c$10F$_t$**). Because 41 of 45 peaks of the diffraction pattern for the (**DSB**/**2F$_c$10F$_t$**) powder with an intensity greater than 1% can be accommodated by the unit cell obtained from the single-crystal study, one can state with confidence that the structure deduced from the small single crystal is indeed representative of the bulk sample characterized by powder diffraction techniques. This level of agreement is repeated for the (**DMADSB**/**2F$_c$10F$_t$**) sample where 34 out of 37 peaks above 4% intensity are successfully indexed. A full listing of the unit cell parameters obtained by the least-squares refinement, the X-ray powder diffraction data, and the de Wolff and Smith-Snyder figures of merit for (**DSB**/**2F$_c$10F$_t$**)and (**DMADSB**/**2F$_c$10F$_t$**) can be found as Supporting Information.

(23) For a discussion of F as a hydrogen bond acceptor, see: Howard, J. A. K.; Hoy, V. J.; O'Hagan, D.; Smith, G. T. *Tetrahedron* **1996**, *52*, 12613.

(24) Thalladi, V. R.; Weiss, H.-H.; Blaser, D.; Boese, R.; Nangia, A.; Desiraju, G. R. *J. Am. Chem. Soc.* **1998**, *120*, 8702.

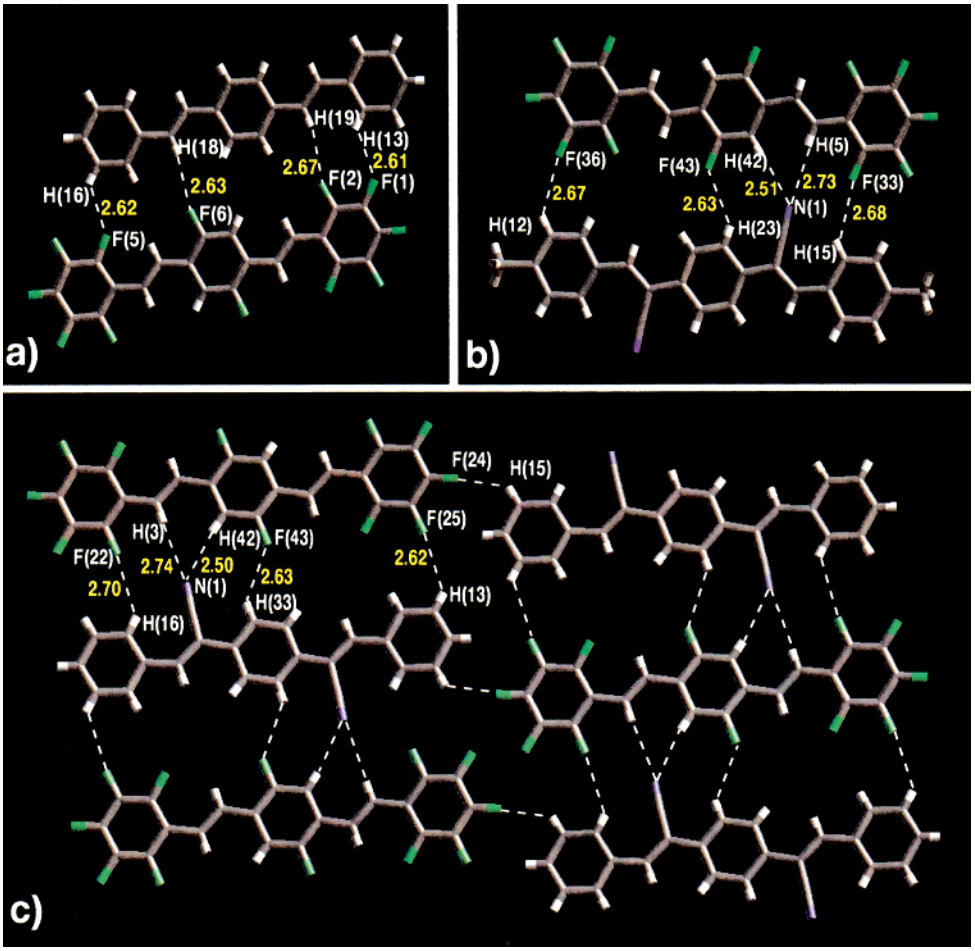

Figure 6. Lateral intermolecular distances under 2.75 Å in a layer of the structure of (a) (**DSB**/**2F$_c$10F$_t$**), (b) (**MeCNDSB**/**2F$_c$10F$_t$**), and (c) (**CNDSB**/**2F$_c$10F$_t$**) viewed roughly perpendicular to the *ac* plane. All distances shown (yellow) are in Å.

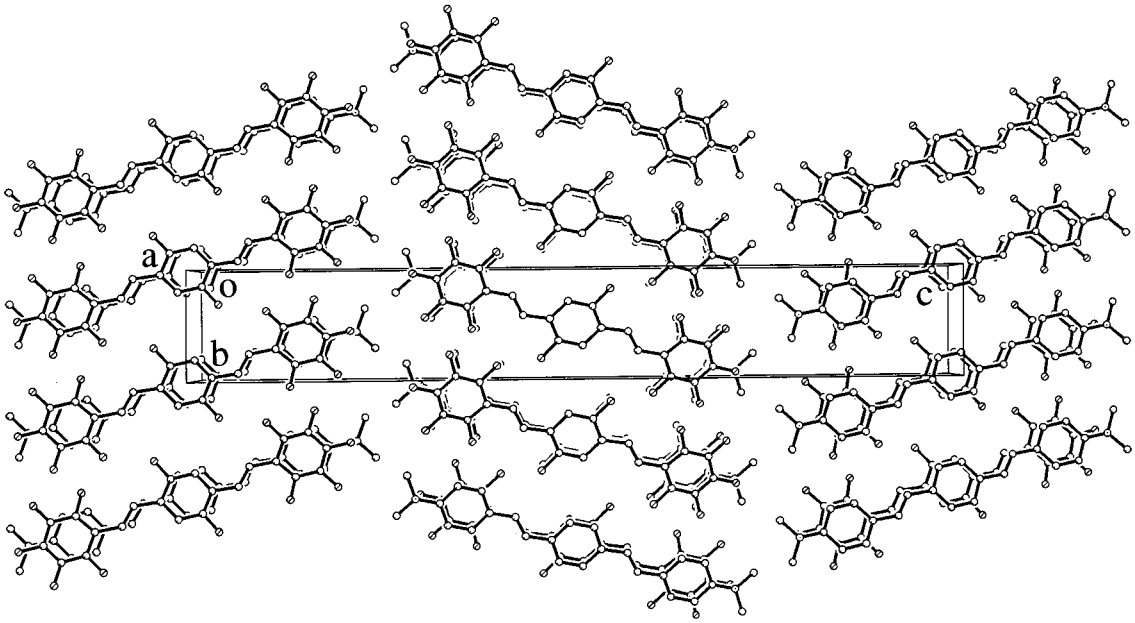

Figure 7. Molecular packing diagram of (**DMADSB**/**2F$_c$10F$_t$**) with a view down the *a* axis.

storage at 4 °C over a period of 2 weeks. The results of this study reveal another pair of molecules stacked face-to-face as shown in Figure 7. The average ring-to-ring distance is 3.42 Å with a transverse slip of 1.43 Å and a longitudinal slip of 0.86 Å. Close H···F contacts between the **DMADSB** and **2F$_c$10F$_t$** partners are again observed between stacks (F(2)···H−C(13), 2.702(6) Å; F(3)···H−C(2), 2.629(6) Å; F(6)···H−C(5), 2.678(6) Å, see Figure 8).

Both **DMADSB** and **2F$_c$10F$_t$** are located at the crystallographic inversion centers. **DMADSB** molecules are located at unit cell body center and at the edge

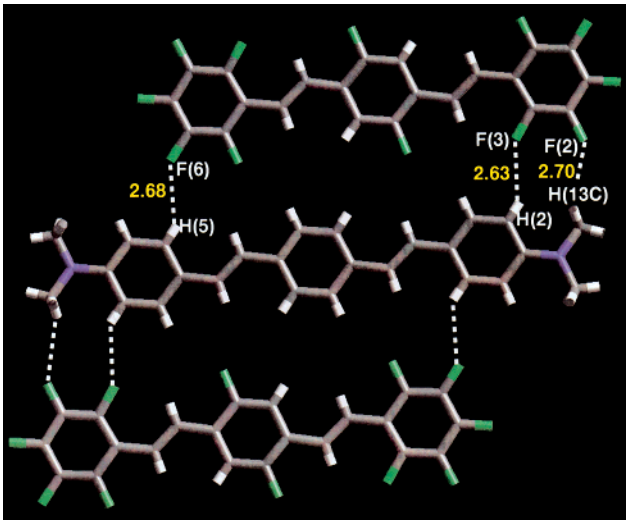

Figure 8. Lateral intermolecular distances ≤2.70 Å in a layer of the structure of (**DMADSB**/**2F$_c$10F$_t$**). All distances shown are in angstroms.

centers of the *a* axis, whereas **2F$_c$10F$_t$** molecules are located at the unit cell origins and at the face centers of the *bc* planes. The long axes of both molecules are aligned approximately along the crystallographic *c* axis and the translation periodicity along the *c* axis is determined by the length of the long molecular axis of **DMADSB** and **2F$_c$10F$_t$**. The *c* axis is slightly more than twice as long as that of the (**DSB**/**2F$_c$10F$_t$**) compound because the adjacent layers in the (**DMADSB**/**2F$_c$10F$_t$**) are not related by the unit cell translational symmetry, as is the case for (**DSB**/**2F$_c$10F$_t$**).

(**DMADSB**/**2F$_c$10F$_t$**) can also be considered to be built from layers stacked along the *c* axis. Within each layer, **DMADSB** and **2F$_c$10F$_t$** form parallel columns similar to those in the (**DSB**/**2F$_c$10F$_t$**) compound. When viewed down the *b* axis, each column consists of molecules of the same type. However, when viewed down the *a* axis, molecules of different types alternate. The most conspicuous difference between (**DSB**/**2F$_c$10F$_t$**) and (**DMADSB**/**2F$_c$10F$_t$**) is the angular relationship between the alternating molecular stacks. In both structures, end contacts are made against the alternate molecule. In (**DSB**/**2F$_c$10F$_t$**), stacks are parallel to each other (Figure 9a). In (**DMADSB**/**2F$_c$10F$_t$**) however, stacks are at an angle of approximately 38° relative to each other. A space-filling extended packing diagram illustrates the pleated stacks of the (**DMADSB**/**2F$_c$10F$_t$**) (Figure 9b).

A single crystal of (**CNDSB**/**2F$_c$10F$_t$**) was obtained from benzene and characterized by XRD (Table 1). Again, the components are stacked face-to-face alternatively as predicted from the electrostatic distribution surfaces of **CNDSB** and **2F$_c$10F$_t$**. A network of H···F contacts is evident as in the previous structures but with an important addition. Within the *ab* layer there is a bifurcated N···H−C bond between **CNDSB** and two sites on **2F$_c$10F$_t$** (N(1) ···H−C(3); 2.74 Å, 158.6° and N(1) ···H−C(42); 2.50 Å, 155.4°). H···F contacts include F(24)···H−C(15) (2.65 Å), F(22)···H−C(16) (2.70 Å), F(25)···H−C(13) (2.62 Å), and F(43)···H−C(33) (2.63 Å) (see Figure 6c). The extended packing closely resembles (**DSB**/**2F$_c$10F$_t$**) with respect to the parallel molecular stacks.

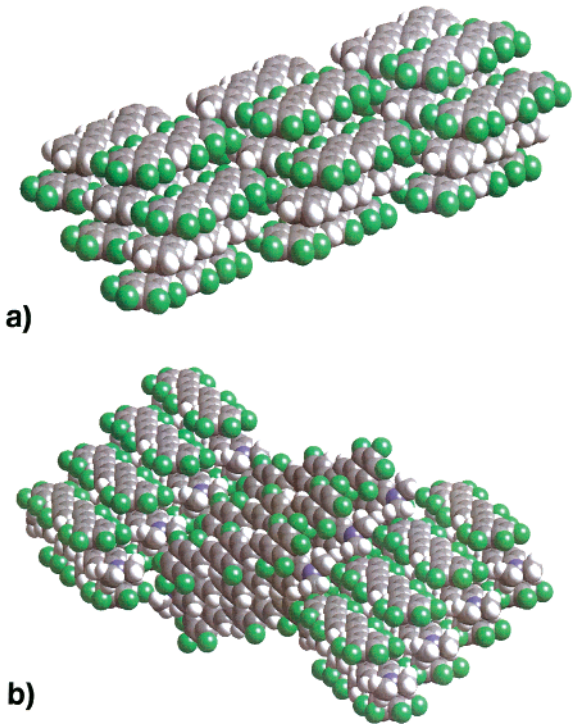

Figure 9. Space-filling extended packing diagram of (a) (**DSB**/**2F$_c$10F$_t$**) and (b) (**DMADSB**/**2F$_c$10F$_t$**) with three layers of cofacial stacks each along the *c* axis.

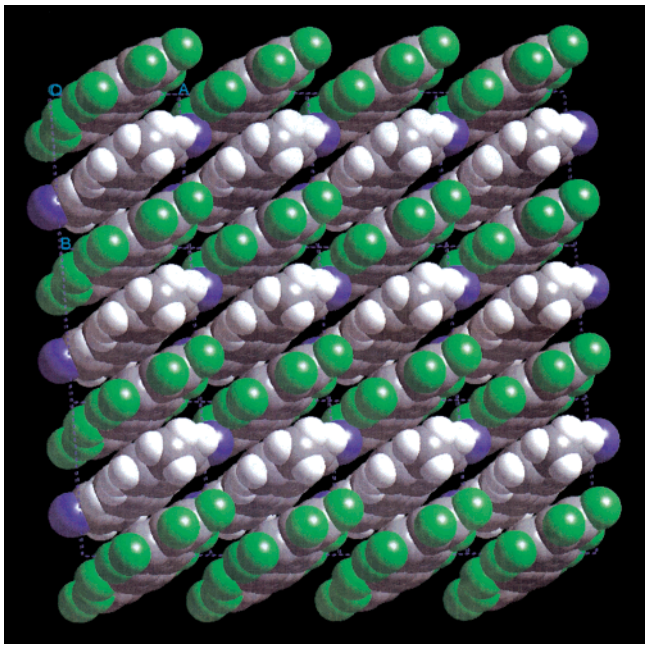

Figure 10. A space-filling diagram of (**MeCNDSB**/**2F$_c$10F$_t$**) with a view perpendicular to the *ab* plane.

A green platelike single crystal of (**MeCNDSB**/**2F$_c$10F$_t$**) suitable for X-ray diffraction was grown in benzene. This structure is very similar to (**DSB**/**2F$_c$10F$_t$**) and (**CNDSB**/**2F$_c$10F$_t$**) even with the addition of the methyl groups at the "para" ends of **MeCNDSB**. Figure 10 provides a view of the cocrystal perpendicular to the *ab* plane. The N of the cyano group again forms a bifurcated contact with hydrogens on **2F$_c$10F$_t$** (N(1)···H−C(5); 2.73 Å, 156.7° and N(1)···H−C(42); 2.51 Å, 156.4°, see Figure 6b). Lateral H···F interactions include F(43)···H−C(23) (2.63 Å), F(33)···H−C(15) (2.68

Table 2. Summary of Differential Scanning Calorimetry Results for (DSB/2F$_c$10F$_t$), (CNDSB/2F$_c$10F$_t$), (MeCNDSB/2F$_c$10F$_t$), and Their Components

compound	T_m (°C)	T_c (°C)
2F$_c$10F$_t$[a]	207	187
DSB[a]	268	261
CNDSB	256	233
MeCNDSB	243	236
(DSB/2F$_c$10F$_t$)	227	222
(CNDSB/2F$_c$10F$_t$)	267	258
(MeCNDSB/2F$_c$10F$_t$)	275	268

[a] T_m and T_c data have been reported for these compounds previously in ref 21.

Å) and F(36)···H−C(42) (2.67 Å). An important difference between this structure and those for (**DSB**/**2F$_c$10F$_t$**) and (**CNDSB/2F$_c$10F$_t$**) is the lack of H···F end contacts. Despite this difference and the additional steric requirements of the methyl group, the parallel packing of alternating molecular columns seen in (**DSB**/**2F$_c$10F$_t$**) and (**CNDSB/2F$_c$10F$_t$**) is conserved.

Structural features and molecular packing modes in (**CNDSB/2F$_c$10F$_t$**) and (**MeCNDSB/2F$_c$10F$_t$**) are strikingly similar to those found in (**DSB/2F$_c$10F$_t$**). In all cases, **2F$_c$10F$_t$** molecules are located at the unit cell origin and **DSB**-type molecules are located at the center of the unit cell *b* axis in the triclinic space group. These three cocrystals have similar unit cell axes and somewhat different unit cell angles. Apparently, substituents such as methyl or cyano groups do not significantly affect the overall molecular packing mode, but steric effects of these substituents lead to noticeable changes in the shape of unit cells.

Differential Scanning Calorimetry (DSC). Table 2 contains a summary of the DSC analysis for the complexes discovered and their components. Analyses of (**CNDSB/2F$_c$10F$_t$**) and (**MeCNDSB/2F$_c$10F$_t$**) show melting points greater than either of their components, as expected for a 1:1 complex of fluorinated/nonfluorinated aromatic pairs.[6,10,13] Because of the high melting point (342 °C) of **DMADSB** and the degree of sublimation of the compound at its melting point, DSC results for **DMADSB** and the corresponding complex could not be obtained reliably.

For (**DSB/2F$_c$10F$_t$**), analyses of two large single crystals of the complex reveal a melting point (228 °C) which is *less* than the T_m of **DSB** (269 °C). This melting transition and the crystallization exotherm are reproducible throughout several heating and cooling cycles and are the only transitions observed (Figure 11). To gain further insight into this low melting transition, an equimolar mixture of **DSB** and **2F$_c$10F$_t$** was encapsulated and analyzed by DSC. The first heating and cooling cycle is shown in Figure 11a. An endotherm corresponding to the melting of **2F$_c$10F$_t$** is observed close to the T_m of the component (207 °C). This weak transition is followed by a strong endotherm, with a T_m that corresponds to the cocrystal. Upon further heating, no transition for **DSB** is observed at 269 °C. Interestingly, the second heating and cooling cycle (Figure 11b) contains only the melting and crystallization that corresponds to the cocrystal. Larger samples of both the complex obtained as crystals and an equimolar mixture of components were heated and cooled in a manner similar to the DSC thermal cycle and then subjected to XRD analysis. Both resulting patterns could be indexed

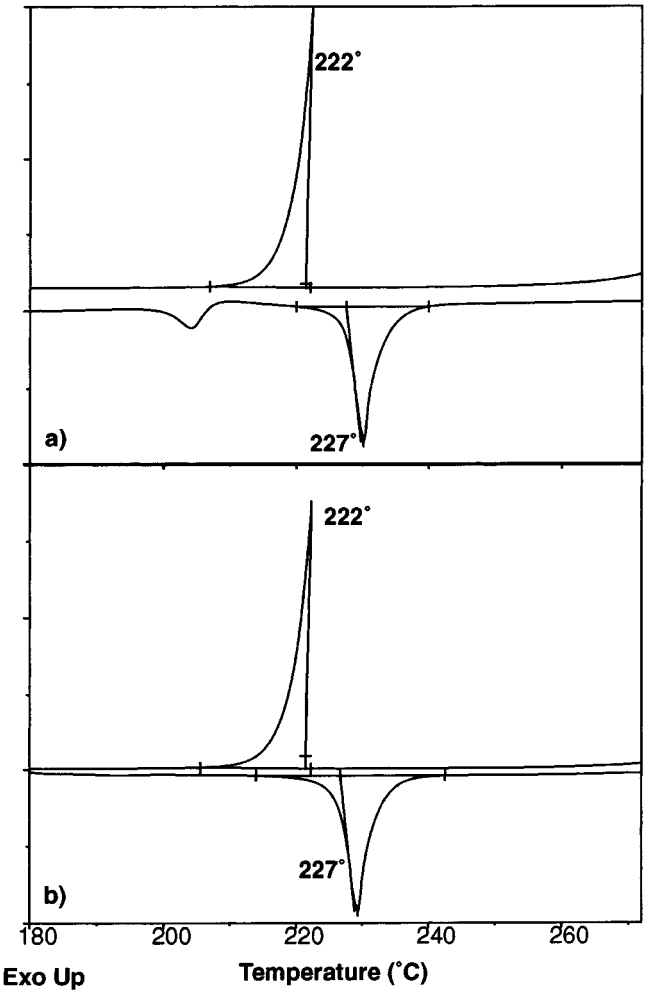

Figure 11. Differential scanning calorimetry trace for an equimolar mixture of DSB and 2F$_c$10F$_t$ for both the (a) first and (b) second heating and cooling cycle.

to the structure determined by the single-crystal diffraction experiment. These data indicate that the sole product from the melt is the cocrystal (**DSB/2F$_c$10F$_t$**).

Conclusion

We have shown that phenyl−perfluorophenyl stacking in combination with H···F contacts can assemble diverse pairs of molecules in the solid state. X-ray powder diffraction can be used in a straightforward manner to identify the formation of binary cocrystals assembled by these relatively weak forces. This approach is similar to Etter's work with cocrystals assembled by strong hydrogen bonding.[20] Although at this time lattice determination still hinges on obtaining suitable single crystals, the success of the powder approach is illustrated by the identification of (**DSB**/**2F$_c$10F$_t$**), (**DMADSB/2F$_c$10F$_t$**), (**CNDSB/2F$_c$10F$_t$**), and (**MeCNDSB/2F$_c$10F$_t$**).

It is interesting that **2F$_c$** and **10F$_t$** do not form a binary cocrystal, despite the similar electrostatic juxtaposition to the (**DSB/2F$_c$10F$_t$**) pair. Figure 1 indicates that for the central ring of **2F$_c$**, inversion of the charge distribution from negative density in the core of the phenyl to positive density, as seen in the central ring of **2F$_c$10F$_t$**, is less than complete. In other words, although the atomic substitution of the (**2F$_c$**/**10F$_t$**) pair

resembles (**DSB**/$2F_c10F_t$), the electronic consequences of the substitution are not the same. In addition, the large number of H···F contacts below 2.75 Å observed in the cocrystals suggest that an optimized H···F registry is important. Electrostatic distributions do not reflect how the molecular topologies of individual components can translate into a three-dimensional H···F network. Finally, the color change observed for the pairs (**DSB**/$2F_c10F_t$) and (**DMADSB**/$2F_c10F_t$) indicates that charge-transfer interactions, where **DSB** and **DMADSB** are donors and $2F_c10F_t$ is the acceptor, may also play a role. It should be noted that for pairs such as benzene/hexafluorobenzene, the intermolecular attractions are thought to be strictly electrostatic in character. For the distyrylbenzene chromophores, the increased electron affinity and lower oxidation potential that accompanies the more delocalized molecular orbitals may allow for a charge-transfer contribution.[25]

Experimental Section

Synthesis. The synthesis of **DSB** and **DMADSB**[26] as well as $2F_c$, $2F_c2F_t$, $2F_c10F_t$,[17] $10F_t$,[6] **CNDSB**, and **MeCNDSB**[16] have been reported previously.

Molecular Modeling. Electrostatic potential maps of **DMADSB**, **CNDSB**, and **MeCNDSB** were calculated using Spartan 5.0.1. Ab initio single-point energy calculations were performed by use of the Hartree−Fock model and the 3-21G* basis set. An electrostatic potential surface was created for the molecule at medium resolution for a density value of 0.002 electrons/au^3.[27] The nitrogen−phenyl bond was constrained to allow the nitrogen lone pair to remain in the plane of the π-system. The electrostatic potential surfaces of the other compounds, reported previously,[17] are included for comparison.

X-ray Powder Diffraction. The X-ray powder diffraction data were collected at room temperature on a Scintag X2 diffractometer operated at 45 kV and 35 mA using Cu radiation. The intensity data were recorded in a continuous mode every 0.02° (2θ) intervals at 2°/min over the range 2−60° (2θ). The software of the diffractometer was used to determine the position of the diffraction maxima, to remove the background, and to eliminate the $K\alpha_2$ component from each reflection. The intensities of the diffraction maxima were measured as peak heights above background and are expressed as a percentage of the strongest peak.

Single-Crystal X-ray Data Collection. The X-ray intensity data were collected on a SMART CCD Area Detector System equipped with a normal focus, 2.4 kW sealed tube X-ray source (Mo Kα radiation, $\lambda = 0.71073$ Å) operated at 45 kV and 40 mA. The temperature control was achieved with an Oxford Cryostream that could provide a temperature range from 80 to 375 K with a stability of about 0.1 K. The empirical absorption corrections based on the equivalent reflections were performed using the program SADABS[28] and other possible effects such as absorption by the glass fiber were simultaneously corrected. The structures were solved by direct methods followed by successive difference Fourier methods. All calculations were performed using SHELXTL[29] (version 5.0.3) running on a Silicon Graphics Indy 5000. Full-matrix refinements were against F^2. Hydrogen atoms were calculated at idealized positions and their atomic positions were refined as riding atoms of their parent carbon atoms. The crystal data and refinement results are summarized in Tables 1 and 2. ORTEP drawings, positional coordinates, selected bond distances, and further details of the data collection, solution, and refinement can be found in the Supporting Information.

Differential Scanning Calorimetry. Differential scanning calorimetry (DSC) was performed on a TA Instruments DSC 2920 Modulated Differential Scanning Calorimeter. Single-component samples (with the exception of $2F_c10F_t$) were encapsulated in aluminum pans and were heated at a rate of 10 °C/min. All other samples were encapsulated in high-pressure capsules and scanned at a rate of 5 °C/min. Melting points were determined by extrapolation to baseline from the slope of the onset of the transition. Heats of fusion were determined by integration of the peak area for the melting transition on the second cycle.

Acknowledgment. Financial support from NSF (DMR 9500627) and the Office of Naval Research is gratefully acknowledged. The authors would like to thank Miguel Delgado and Graciela Diaz de Delgado for useful discussions and Rene Lachicotte for help with the crystal structure of (**DSB**/$2F_c10F_t$).

Supporting Information Available: Complete details for the crystallographic studies of all complexes reported, additional powder diffraction figures, and details of powder diffraction data indexing (PDF). This information is available free of charge via the Internet at http://pubs.acs.org.

CM990608A

(25) Turro, N. J. *Modern Molecular Photochemistry* University Science Books: Sausalito, CA 1991.
(26) Heller, A. *J. Chem. Phys.* **1964**, *40*, 2839.
(27) Hehre, W. J. *Practical Strategies for Electronic Structure Calculations*; Wavefunction: Irvine, CA, **1995**; p 205.
(28) Sheldrick, G. M. *SADABS User Guide*; University of Göttingen: Germany, 1995. The SADABS program is based on the method of Blessing; see: Blessing, R. H. *Acta Crystallogr.* **1995**, *51*, 33.
(29) ***SHELXTL:*** *Structure Analysis Program, version 5.04*; Siemens Industrial Automation Inc.: Madison, WI, 1995.